RESEARCH ARTICLE SUMMARY

METABOLISM

Aster-dependent nonvesicular transport facilitates dietary cholesterol uptake

Alessandra Ferrari, Emily Whang, Xu Xiao, John P. Kennelly, Beatriz Romartinez-Alonso, Julia J. Mack, Thomas Weston, Kai Chen, Youngjae Kim, Marcus J. Tol, Lara Bideyan, Alexander Nguyen, Yajing Gao, Liujuan Cui, Alexander H. Bedard, Jaspreet Sandhu, Stephen D. Lee, Louise Fairall, Kevin J. Williams, Wenxin Song, Priscilla Munguia, Robert A. Russell, Martin G. Martin, Michael E. Jung, Haibo Jiang, John W. R. Schwabe, Stephen G. Young, Peter Tontonoz*

INTRODUCTION: Hypercholesterolemia is a major risk factor for cardiovascular disease. The small intestine is the gatekeeper of dietary cholesterol absorption and a tractable target for lipid-lowering therapies. Niemann-Pick C1 Like 1 (NPC1L1), the target of the hypocholesterolemic drug ezetimibe (EZ), facilitates the deposition of dietary cholesterol from the gut lumen into the apical plasma membrane (PM) of enterocytes. Subsequently, cholesterol moves to the endoplasmic reticulum (ER) where it is esterified by ACAT2. Cholesterol ester is packaged into chylomicrons for release into the circulation and delivery to tissues. How cholesterol moves from the brush border of enterocytes to the ER, however, has been a longstanding question.

RATIONALE: Prior studies have proposed that endosomal pathways, possibly involving NPC1L1, may contribute to the movement of cholesterol into enterocytes. However, the involvement of nonvesicular pathways has not been tested. Aster proteins are ER-resident nonvesicular transporters that bind cholesterol and facilitate its removal from the PM by forming PM-ER contact sites. We addressed the role of Asters in intestinal physiology and systemic cholesterol homeostasis using cellular assays, intestinal enteroid cultures, structural biology, and genetically modified mouse models.

RESULTS: We discovered that Aster-B is translocated to the brush border of enterocytes of the small intestine in response to oral administration of cholesterol to mice. Since Aster-B and Aster-C are expressed in the small intestine, we generated mice with genetic deletions of both proteins. Loss of Aster-dependent nonvesicular cholesterol transport in enterocytes compromised dietary cholesterol absorption, despite the presence of NPC1L1. We used intestinal enteroid cultures to demonstrate that Aster deletion caused an accumulation of ALOD4-binding accessible cholesterol at the PM of enterocytes, indicative of impaired cholesterol movement to the ER. Mice lacking Asters also showed evidence of ER cholesterol depletion, including reduced cholesterol ester formation and activation of the SREBP2 transcriptional program for de novo cholesterol synthesis. Aster-deficient mice produced chylomicrons depleted of cholesterol esters and were protected from diet-induced hypercholesterolemia. Both Aster-B and Aster-C bound EZ, and we resolved the crystal structure of the Aster-C-EZ complex to 1.6 Å resolution. Based on this observation, we examined potential cooperation between Asters and NPC1L1. We showed that NPC1L1, by saturating the brush border with diet-derived cholesterol, was necessary for Aster recruitment to the apical PM of enterocytes. Acting downstream of NPC1L1, Asters were required to move cholesterol deposited by NPC1L1 to the enterocyte ER. Finally, the small-molecule Aster inhibitor AI-3d caused the accumulation of accessible cholesterol at the PM of both mouse and human intestinal enteroids and reduced dietary cholesterol absorption in mice.

CONCLUSION: Asters and NPC1L1 perform sequential, nonredundant functions in dietary cholesterol uptake. Nonvesicular cholesterol transport mechanisms downstream of NPC1L1 action at the PM are important for cholesterol movement in enterocytes and contribute to systemic sterol homeostasis. These findings highlight the Aster pathway as a physiologically important determinant of dietary lipid absorption that can be targeted pharmacologically. ■

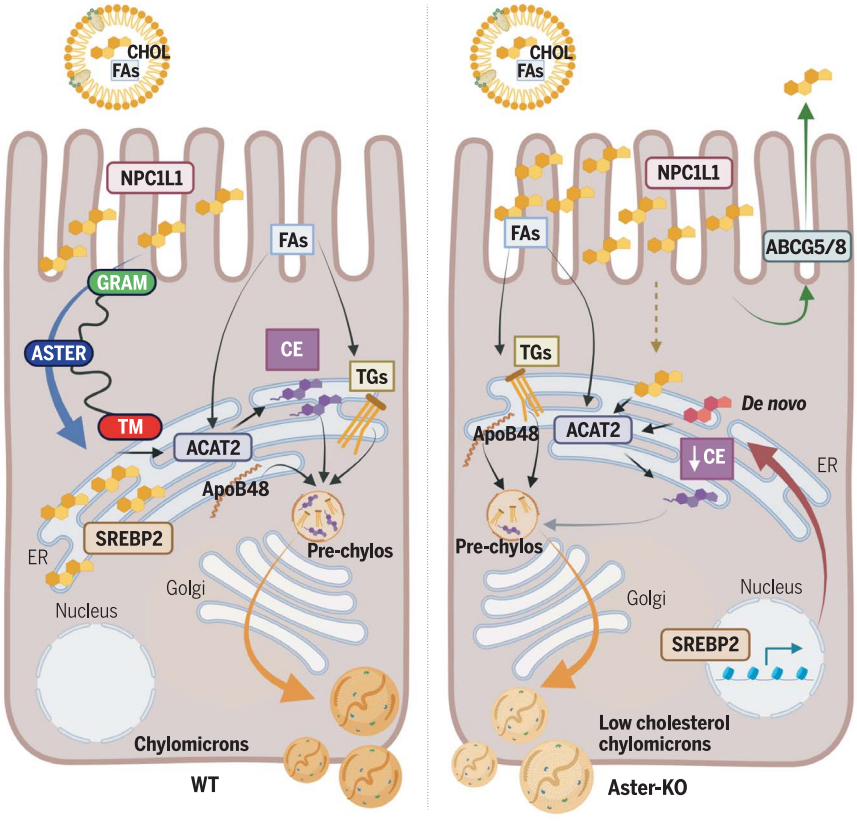

Asters facilitate intracellular movement of dietary cholesterol in enterocytes. NPC1L1 mediates the deposition of dietary cholesterol at the brush border, thus recruiting Asters to form PM-ER contact sites. Asters subsequently facilitate the nonvesicular movement of cholesterol to ER for esterification. Deletion of Asters causes ER sterol depletion, activation of SREBP2, production of chylomicrons depleted of cholesterol esters, and reduced systemic cholesterol burden. [Figure created using BioRender]

The list of author affiliations is available in the full article.
*Corresponding author. Email: ptontonoz@mednet.ucla.edu
Cite this article as A. Ferrari *et al.*, *Science* **382**, eadf0966 (2023). DOI: 10.1126/science.adf0966

READ THE FULL ARTICLE AT
https://doi.org/10.1126/science.adf0966

RESEARCH ARTICLE

METABOLISM

Aster-dependent nonvesicular transport facilitates dietary cholesterol uptake

Alessandra Ferrari[1,2]†, Emily Whang[1,2,3]†, Xu Xiao[1,2], John P. Kennelly[1,2], Beatriz Romartinez-Alonso[4], Julia J. Mack[5], Thomas Weston[5,6], Kai Chen[7,8], Youngjae Kim[9], Marcus J. Tol[1,2], Lara Bideyan[1,2], Alexander Nguyen[1,2,10], Yajing Gao[1,2], Liujuan Cui[1,2], Alexander H. Bedard[1,2], Jaspreet Sandhu[1,11], Stephen D. Lee[1,2], Louise Fairall[4], Kevin J. Williams[2,12], Wenxin Song[5,6], Priscilla Munguia[5,6], Robert A. Russell[13], Martin G. Martin[3], Michael E. Jung[9], Haibo Jiang[7,8], John W. R. Schwabe[4], Stephen G. Young[5,6], Peter Tontonoz[1,2]*

Intestinal absorption is an important contributor to systemic cholesterol homeostasis. Niemann-Pick C1 Like 1 (NPC1L1) assists in the initial step of dietary cholesterol uptake, but how cholesterol moves downstream of NPC1L1 is unknown. We show that Aster-B and Aster-C are critical for nonvesicular cholesterol movement in enterocytes. Loss of NPC1L1 diminishes accessible plasma membrane (PM) cholesterol and abolishes Aster recruitment to the intestinal brush border. Enterocytes lacking Asters accumulate PM cholesterol and show endoplasmic reticulum cholesterol depletion. Aster-deficient mice have impaired cholesterol absorption and are protected against diet-induced hypercholesterolemia. Finally, the Aster pathway can be targeted with a small-molecule inhibitor to manipulate cholesterol uptake. These findings identify the Aster pathway as a physiologically important and pharmacologically tractable node in dietary lipid absorption.

The intestine regulates systemic lipid homeostasis by gating dietary cholesterol intake (*1*). Cholesterol is absorbed by enterocytes and packaged into chylomicrons, which are released into the lymphatics and ultimately reach the systemic circulation (*2*). Most of the cholesterol in chylomicrons is esterified, and cholesterol ester (CE) is necessary for chylomicron packaging. Free cholesterol deposited into the inner leaflet of the apical plasma membrane (PM) by Niemann-Pick C1-Like 1 (NPC1L1) must subsequently move to the ER to be esterified by ACAT2 (*3*–*5*). NPC1L1 is an important mediator of intestinal cholesterol uptake (*6*, *7*), but how cholesterol is delivered to the enterocyte ER for esterification remains unknown.

NPC1L1 is a target of the drug ezetimibe (EZ) (*8*–*10*). The combination of EZ and a statin further reduces cardiovascular events compared with statin alone (*10*), validating the intestine as a therapeutic target for the regulation of cholesterol homeostasis. EZ was initially discovered to be an inhibitor of ACAT2 (*11*). Its notable effects on cholesterol absorption led to its FDA approval even before it was found that it inhibits NPC1L1. Genetic ablation of NPC1L1 or EZ administration impairs cholesterol absorption (*6*). Treatment with EZ protects mice from diet-induced hypercholesterolemia and atherosclerosis (*1*, *3*, *12*, *13*). Structural analyses have revealed that the N-terminal domain of NPC1L1 contains a cavity that accommodates cholesterol (*14*–*16*). Cholesterol moves through this channel to diffuse into the lipid bilayer. EZ binds within the channel, thereby blocking cholesterol deposition. Despite the importance of the NPC1L1-ACAT2 axis for cholesterol homeostasis, how cholesterol received by NPC1L1 at the PM ultimately reaches the ER is unknown (*17*–*24*).

Aster proteins (Aster-A, -B, and -C, encoded by *Gramd1a, Gramd1b,* and *Gramd1c*, respectively) bind cholesterol and facilitate its movement between membranes (*25*–*27*). Members of this family have a central cholesterol-binding pocket that is flanked by a GRAM domain at the N terminus and an ER transmembrane domain at the C terminus. The GRAM domain binds the PM in response to cholesterol loading, allowing Asters to transfer cholesterol down a concentration gradient from the PM to the ER. The role of nonvesicular cholesterol transport in cell function is highly cell-type specific. In mice, Aster-B is required for CE storage and corticosteroid synthesis in the adrenal cortex (*25*), whereas Aster-C is important for hepatic reverse cholesterol transport (*28*).

We show that NPC1L1 and Asters play sequential, nonredundant roles in the delivery of dietary cholesterol from the intestinal lumen to the enterocyte ER. Asters are recruited to the enterocyte PM upon cholesterol loading, and loss of their expression impairs CE production. Treatment of mice with a small-molecule Aster inhibitor reduces the systemic absorption of dietary cholesterol, and mice lacking Asters in the intestine are protected from diet-induced hypercholesterolemia. Our findings support a model in which the principal function of NPC1L1 is to enrich the enterocyte PM with dietary cholesterol. This enrichment facilitates the recruitment of Asters to the PM where they mediate nonvesicular cholesterol trafficking to the ER. These findings identify intestinal Asters as key players in dietary lipid absorption and potential targets for the control of cholesterol homeostasis.

Results

Intestinal Aster expression is regulated by liver x receptors

Transcripts for Aster-A, -B, and -C are expressed in the small intestine (SI) (Fig. 1A), and RNA-seq from proximal jejunal scrapings of C57BL6/J mice confirmed robust expression of *Gramd1b* and *Gramd1c* and low expression of *Gramd1a* (fig. S1A). The most abundant *Gramd1c* transcript in the SI encodes a truncated Aster-C lacking the N-terminal GRAM domain. RNA-seq also revealed the presence of two transcripts for *Gramd1b* in the intestine; one was the same as that identified previously in macrophages (*25*), while the other had an extended N-terminal region upstream of the GRAM domain (fig. S1A). An intestine-specific promoter in the *Gramd1b* locus (chr9: 40465470-40465756) defined the longer variant. Absolute quantification of *Gramd1* transcripts in intestinal samples confirmed that those for Aster-B and -C were most abundant (fig. S1B). Aster-B was expressed along the entire length of the SI (duodenum to the ileum) (fig. S1C). In Caco-2 cells, transcripts for Aster-B and -C were induced upon differentiation (fig. S1D). Liver x receptor transcription factors are key regulators of cholesterol metabolism (*29*, *30*). Treatment of wild-type (WT) mice with the LXR agonist GW3965 induced the expression of all three Asters in the SI (fig. S1E), consistent with a role for the Aster pathway in intestinal cholesterol flux.

[1]Department of Pathology and Laboratory Medicine, University of California, Los Angeles, Los Angeles, CA 90095, USA. [2]Department of Biological Chemistry, University of California, Los Angeles, Los Angeles, CA 90095, USA. [3]Pediatric Gastroenterology, Hepatology, and Nutrition, David Geffen School of Medicine, University of California, Los Angeles, Los Angeles, CA 90095, USA. [4]Institute for Structural and Chemical Biology, University of Leicester, Leicester LE1 7RH, UK. [5]Department of Medicine, Division of Cardiology, University of California, Los Angeles, Los Angeles, CA, 90095, USA. [6]Department of Human Genetics, University of California, Los Angeles, Los Angeles, CA 90095, USA. [7]Department of Chemistry, The University of Hong Kong, Hong Kong 999077, China. [8]School of Molecular Sciences, The University of Western Australia, Crawley, WA 6009, Australia. [9]Department of Chemistry, University of California, Los Angeles, Los Angeles, CA 90095, USA. [10]Vatche and Tamar Manoukian Division of Digestive Diseases, Department of Medicine David Geffen School of Medicine, University of California, Los Angeles, Los Angeles, CA 90095, USA. [11]Molecular Biology Institute, University of California, Los Angeles, Los Angeles, CA 90095, USA. [12]UCLA Lipidomics Core, University of California, Los Angeles, Los Angeles, CA 90095, USA. [13]National Deuteration Facility, Australian Nuclear Science and Technology Organisation, Lucas Heights, NSW 2234, Australia.
***Corresponding author. Email: ptontonoz@mednet.ucla.edu**
†These authors contributed equally to this work.

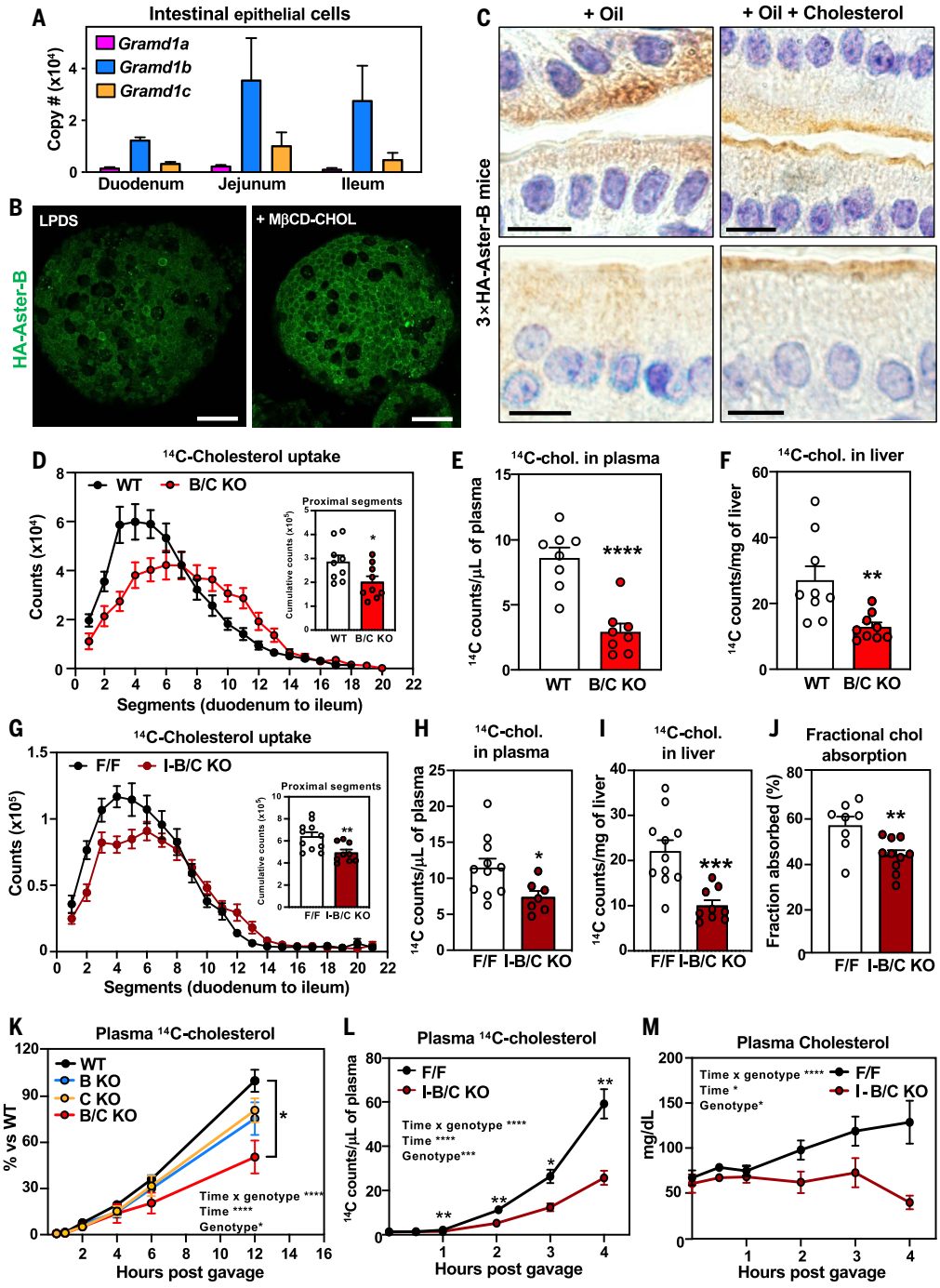

Fig. 1. Aster proteins modulate dietary cholesterol uptake. (**A**) Absolute quantification of *Gramd1a/b/c* mRNA in the duodenum, jejunum, and ileum of C57BL/6J male mice (n = 5). (**B**) IF microscopy of HA-Aster-B in intestinal organoids from 3×HA-Aster-B mice during sterol deprivation (left) or loading with MβCD-cholesterol (right). Scale bar is 50 µm. (**C**) Immunohistochemical staining of HA-Aster-B in small intestines from 3×HA-Aster-B mice after a gastric gavage with corn oil or corn oil with cholesterol. For upper and lower panels, scale bar is 20 and 10 µm, respectively. (**D**) Radioactivity in intestinal segments of female WT and B/C KO mice after oral gavage with olive oil containing [^{14}C] cholesterol for 2 hours (n = 9 per group), and cumulative counts in the proximal intestine. (**E**) Radioactivity in plasma of mice described in (D). (**F**) Radioactivity in livers of mice described in (D). (**G**) Radioactivity in intestinal segments of female F/F and I-B/C KO mice after an oral challenge of olive oil containing [^{14}C] cholesterol for 2 hours (n = 9 per group), and cumulative counts in the proximal intestine. (**H**) Radioactivity in plasma of mice described in (H). (**I**) Radioactivity in livers of mice described in (I). (**J**) Cholesterol absorption measured by the fecal dual-isotope ratio method (n = 8 to 10 per group). (**K**) Kinetics of radioactivity in plasma of female WT (n = 9), BKO (n = 5), CKO (n = 5), B/C KO (n = 5) mice after an oral challenge of olive oil containing [^{14}C]cholesterol. (**L**) Kinetics of radioactivity in plasma of female F/F and I-B/C KO mice after injection of Poloxamer-407 and an oral challenge of [^{14}C]cholesterol in olive oil. (**M**) Kinetics of total cholesterol in mice described in (L). Data are expressed as mean ± SEM. Statistical analysis: unpaired t test for (D, E, F, G, H, I, and J); 2-way analysis of variance (ANOVA) with Tukey's multiple comparisons test for (K); and 2-way ANOVA with Sidak's multiple comparisons test for (L and M). *P < 0.05, **P < 0.01, ***P < 0.001, ****P < 0.0001.

Aster proteins facilitate cholesterol uptake in the small intestine

To visualize endogenous Aster-B movement in enterocytes, we used CRISPR-Cas9 editing to insert a 3×HA tag into the mouse *Gramd1b* locus (fig. S1, F and G). Immunohistochemistry of intestinal tissue revealed that HA-Aster-B was enriched in the villi of the jejunum with lower expression in the crypts (fig. S1H). To study Aster localization in culture we derived enteroids from intestinal crypts of HA-Aster-B mice. Confocal imaging demonstrated that Aster-B was recruited to the PM in response to loading with methyl-β-cyclodextrin (MβCD)–cholesterol (Fig. 1B). Accordingly, immunohistochemistry showed a greater distribution of HA-Aster-B at the brush border of enterocytes 1 hour after intra-gastric gavage with cholesterol in corn oil versus corn oil alone (Fig. 1C).

To explore the function of Asters in intestinal physiology, we generated global knockout mice for Aster-B (B-KO), Aster-C (C-KO), or both (B/C-KO) (fig. S2, A and B). Deletion of Asters was verified in jejunal scrapings (fig. S2, C, D, and E). The SI from B/C-KO mice had no obvious histological abnormalities (fig. S2F), and body weight and intestinal length showed minimal differences across genotypes (fig. S2G). To evaluate the role of Asters in cholesterol uptake, we administered [^{14}C]cholesterol by gastric gavage and measured radioactivity in SI 2 hours later. No differences in [^{14}C]cholesterol absorption were detected in single-KO mice (fig. S2, H to M), but we observed markedly reduced absorption in the proximal intestine of B/C-KO mice (Fig. 1D and fig. S2, N and O). B/C-KO mice also had reduced amounts of [^{14}C]cholesterol in the plasma and liver 2 hours after gavage (Fig. 1, E and F).

To confirm that this impairment in cholesterol absorption resulted from Aster deficiency in enterocytes, we generated mice with tamoxifen-inducible, intestine-specific deletion of Aster-B (I-B-KO), Aster-C (I-C-KO), or both (I-B/C-KO) by intercrossing double "floxed" mice with Villin-Cre^{ERT2} transgenic mice (fig. S3, A to F). I-B/C KO mice displayed normal crypt cell proliferation as revealed by OLFM4 staining (fig. S3G). Minimal differences in body weight or SI length were observed between control and I-B/C KO mice (fig. S3H). Thus, loss of Aster expression does not appear to compromise intestinal development.

Cholesterol uptake was similar in I-B KO, I-C-KO, and littermate control mice (fig. S3, I to N). However, I-B/C-KO mice had reduced [^{14}C]cholesterol absorption compared with floxed controls (similar to global B/C-KO mice) (Fig. 1, G to I). Cumulative counts in the proximal tract (Fig. 1G) were reduced, whereas counts in medial and distal regions were not different (fig. S3, O and P). Fractional cholesterol absorption, assessed by fecal dual isotope labeling, confirmed impaired cholesterol absorption in I-B/C-KO mice (Fig. 1J). By contrast, there were no detectable reductions in ^{14}C counts in intestinal segments, plasma, and liver of I-B/C-KO mice after oral gavage of [^{14}C]triolein (fig. S4, A to D). Glucose absorption was not affected in I-B/C-KO mice (fig. S4E). Thus, loss of Aster function in enterocytes selectively impairs cholesterol absorption.

Next, we followed the appearance of orally administered [^{14}C]cholesterol in the plasma over 12 hours. There was a marked reduction in ^{14}C counts in the plasma of B/C-KO mice, whereas B-KO and C-KO mice exhibited an intermediate phenotype (Fig. 1K). We also injected mice with the lipoprotein lipase inhibitor Poloxamer-407, gavaged them with [^{14}C]cholesterol, and collected plasma up to 4 hours post gavage. The appearance of [^{14}C]cholesterol in the plasma over time, as well as total plasma cholesterol levels, was reduced in I-B/C-KO mice (Fig. 1, L and M).

Nonvesicular cholesterol transport enables intestinal CE production

Adequate CE is required for chylomicron production by the intestine. We hypothesized that Aster-mediated nonvesicular transport from the PM to the ER facilitates cholesterol esterification and subsequent incorporation into chylomicrons. We used nanoscale secondary ion mass spectrometry (NanoSIMS) imaging to visualize cholesterol uptake and intracellular distribution by enterocytes (*31*, *32*). Mice received an intra-gastric gavage of [^{13}C]fatty acids and [^{2}H]cholesterol in olive oil. Biopsies from the duodenum were harvested 2 hours later. Backscattered electron images of duodenal sections verified the integrity of intestinal villi (Fig. 2A and fig. S5A). NanoSIMS images of the same sections (Fig. 2A and fig. S5A) revealed reduced amounts of ^{2}H in medial and distal segments of the duodenum in B/C-KO mice. Quantification of $^{13}C^-$ and $^{2}H^-$ secondary ions confirmed reduced cholesterol uptake by enterocytes lacking Asters (Fig. 2B and fig. S5B).

Previous studies showed that in macrophages (*33*) and hepatocytes (*28*) Asters specifically recognize the accessible pool of PM cholesterol (*34*, *35*). To prove that Asters transfer accessible cholesterol from the PM to ER in intestinal epithelial cells, we stained WT and Aster-B/C KO enteroids with ALOD4, a bacterial peptide that selectively binds to accessible cholesterol. Confocal microscopy revealed enhanced ALOD4 staining at the PM of Aster-B/C KO enteroids loaded with MβCD-cholesterol (Fig. 2C), consistent with reduced cholesterol movement to the ER. Accordingly, lipidomic analysis of jejunal scrapings revealed reduced CE in B/C-KO mice after feeding (Fig. 3A). Other lipid species were not affected by Aster deficiency (fig. S6A). Consistent with these findings, ^{14}C-labeled CE accumulation was reduced in the proximal jejunum of Aster-deficient mice 2 hours after oral administration of [^{14}C]cholesterol in olive oil (Fig. 3B). The level of free [^{14}C]cholesterol was similar between groups (fig. S6B). SREBP-2 target gene expression was higher in global B/C-KO than in WT mice, both in fasted and refed states (Fig. 3, C and D), consistent with reduced ER cholesterol. Similar findings were observed in jejunal scrapings of I-B/C-KO mice (Fig. 3E). Protein levels of SREBP-2 targets in duodenal scrapings were correspondingly elevated in B/C-KO mice (Fig. 3F). We also observed up-regulation of *Srebf2* and its targets in jejunal scrapings in B/C-KO mice fed a high-cholesterol (HC) diet (1.25% cholesterol) (fig. S6C). Thus, even in the setting of increased dietary cholesterol, cholesterol synthesis was activated in B/C-KO mice. We did not observe changes in SREBP-2 pathway expression in the jejunum of global (fig. S6, D and E) or intestinal-specific (fig. S6, F and G) single-KO mice.

Plasma levels of ApoB48 after refeeding with a HC diet were not different between groups (Fig. 3, G and H), despite lower plasma cholesterol levels in I-B/C KO mice (Fig. 3I). Plasma triglyceride levels were also comparable (fig. S6H), consistent with our observation that fatty acid absorption was unaffected by loss of Asters (fig. S4, A to D). These findings suggest that Aster deficiency reduces cholesterol content in chylomicrons, but does not alter the process of chylomicron assembly and release per se. In support of this conclusion, there were fewer ^{14}C counts in the chylomicron fraction of plasma isolated 2 hours after oral gavage of [^{14}C]cholesterol in I-B/C KO mice versus control mice (Fig. 3J). To show that this decrease in cholesterol was due to a reduction in CE, we analyzed chylomicron composition in mice gavaged with d4-cholesterol and injected with Poloxamer-407. I-B/C KO mice had reduced d4-CE in chylomicrons (Fig. 3K) without changes in d4-cholesterol compared with floxed control mice (Fig. 3L). Unlabeled CE species were also lower whereas unlabeled cholesterol was not different (fig. S6, I and J).

Loss of Asters protects against diet-induced hypercholesterolemia

Next, we investigated whether intestinal Aster deficiency affected systemic cholesterol homeostasis. After 21 days of an HC diet we observed a modest decrease in the weight of global B/C-KO mice (Fig. 4A), accompanied by reduced fasting plasma cholesterol levels (Fig. 4B). Liver cholesterol levels were also reduced (Fig. 4C). We also found lower fasting plasma cholesterol levels in intestine-specific Aster-KO mice but no change in body weight (Fig. 4, D and E). FPLC fractionation of plasma revealed lower cholesterol levels in the VLDL/LDL and HDL fractions from Aster-KO mice (Fig. 4F). Plasma

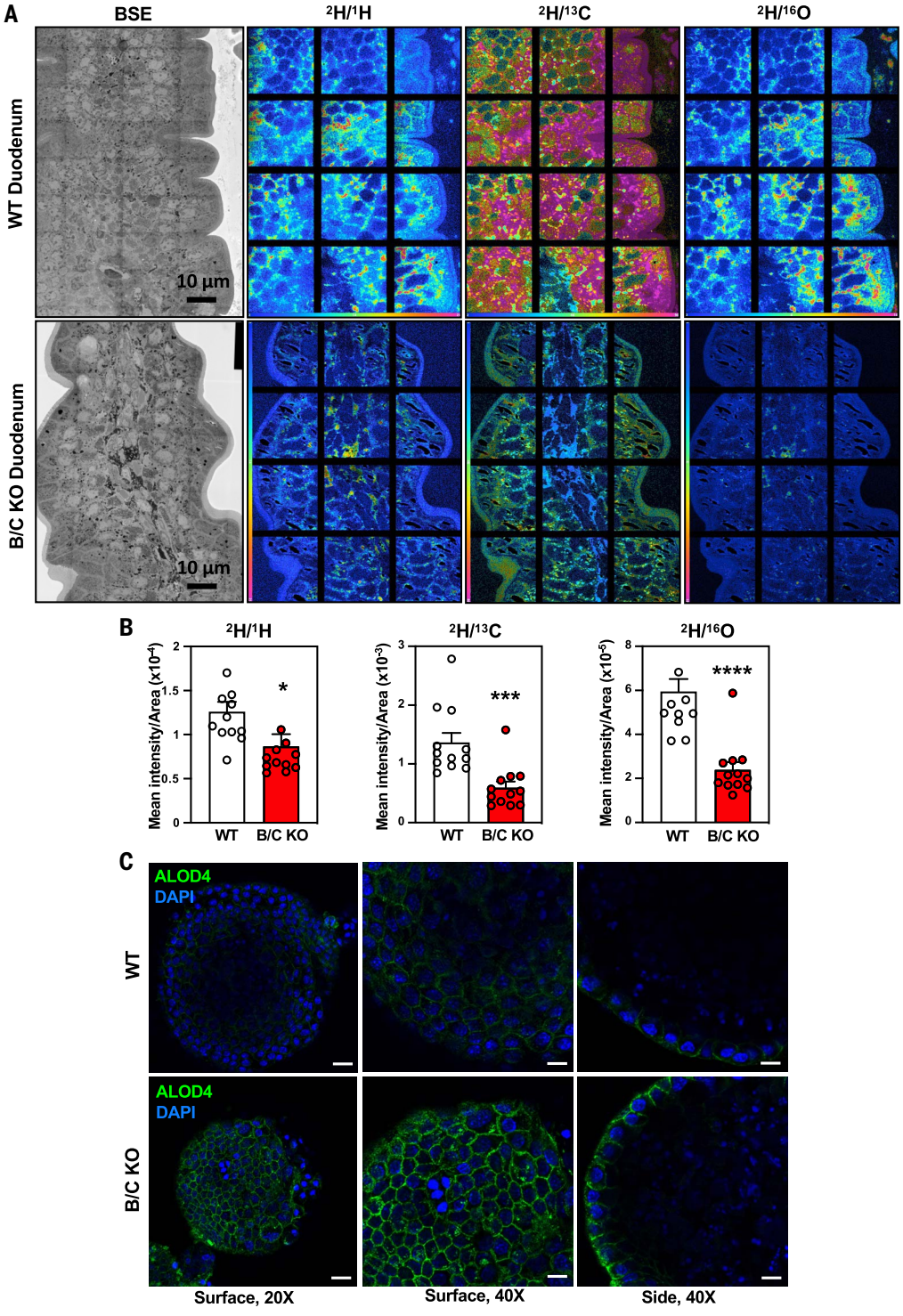

Fig. 2. Deletion of Asters reduces cholesterol internalization from the plasma membrane. (**A**) Backscattered electron images and NanoSIMS images of a mid-duodenum villus from WT and B/C KO mice. (**B**) Quantification of the $^{2}H^{-}$ secondary ion signal, normalized to the $^{1}H^{-}$, $^{13}C^{-}$, and $^{16}O^{-}$ signals. (**C**) ALOD4 imaging of murine enteroids from WT and B/C KO mice 2 hours after loading with MβCD cholesterol. For left panels, scale bar is 20 µm. For middle and right panels scale bar is 10 µm. Data are expressed as mean ± SEM. Statistical analysis: unpaired *t* test; **P* < 0.05, ****P* < 0.001, *****P* < 0.0001.

triglyceride levels were similar between groups (fig. S7, A and B). SREBP-2 pathway gene and protein expression (Fig. 4, G to I) was elevated in global B/C-KO and I-B/C-KO mice compared with controls. Thus, de novo cholesterol synthesis was activated in the KO intestine even in the setting of excess dietary cholesterol (Fig. 4, H and I). Lipidomic analyses revealed reduced CE in I-B/C-KO enterocytes on the HC diet (Fig. 4J), without changes in other lipid species (fig. S7C). We did not observe changes in body weight (fig. S7D) or lipid levels in Aster single-KO mice after 21 days of the HC diet (fig. S7, E and F), nor did we observe a change in SREBP-2 targets (fig. S7G).

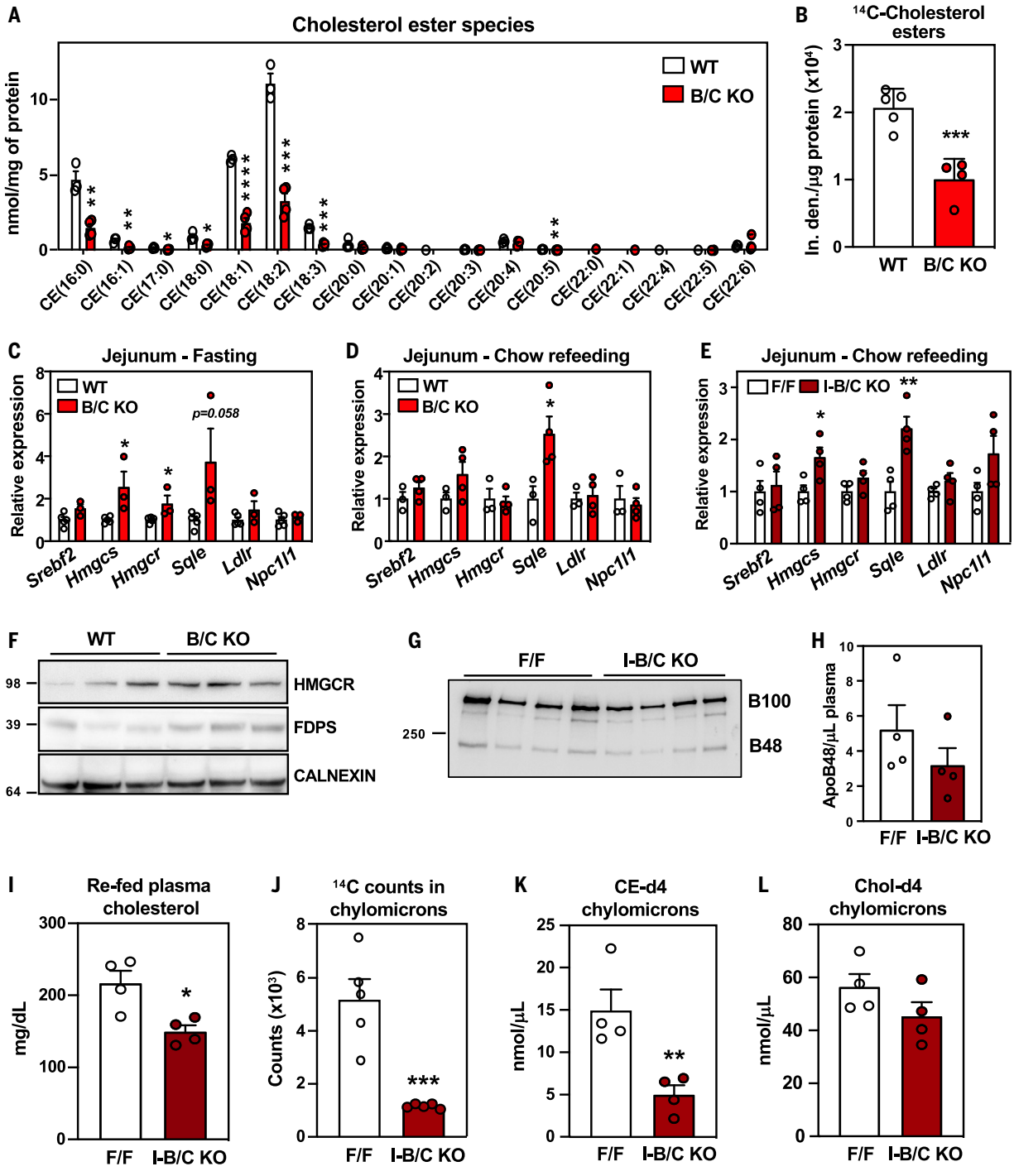

Fig. 3. Loss of Asters in intestine impairs cholesterol transfer to the ER. (**A**) Cholesterol ester quantification by mass spectrometry in proximal jejunum from WT (n = 3) and B/C KO (n = 4) 2 hours after refeeding a chow diet following a 10-hour fast. (**B**) Quantification of ^{14}C-labeled CE isolated from proximal jejunum scrapings of WT (n = 5) and B/C KO (n = 4) mice 2 hours after oral gavage of [^{14}C]cholesterol. (**C**) Gene expression from distal jejunum scrapings of WT (n = 5) and B/C KO (n = 3) mice after 4 hours of fasting. (**D**) Gene expression from distal jejunum scrapings of WT (n = 3) and B/C KO (n = 4) mice 2 hours after refeeding chow diet following a 10-hour fast. (**E**) Gene expression from distal jejunum scrapings of F/F (n = 4) and I-B/C KO (n = 4) mice 2 hours after refeeding chow diet following a 10-hour fast. (**F**) Western blot analysis of duodenum scrapings of mice described in (D). (**G**) Western blot analysis and quantification of plasma from F/F (n = 4) and I-B/C KO (n = 4) mice fed for 21 days a high cholesterol (1.25%) diet, after a 10-hour fast followed by 2 hours of refeeding a HC diet. (**H**) ApoB48 quantified by densitometry and normalized on the volume of plasma used for WB detection. (**I**) Plasma cholesterol of mice described in (G). (**J**) Quantification of ^{14}C-counts in chylomicrons isolated from plasma of F/F (n = 5) and I-B/C KO (n = 5) 3 hours after treatment with Poloxamer-407 and oral gavage of [^{14}C]cholesterol. (**K**) and (**L**) Quantification of deuterated (-d4) CE (K) and free cholesterol (L) in chylomicrons isolated from plasma of F/F (n = 4) and I-B/C KO (n = 4) 3.5 hours after treatment with Poloxamer-407 and oral gavage with cholesterol-d4. Data are expressed as mean ± SEM. Statistical analysis: unpaired t test, *P < 0.05, **P < 0.01, ***P < 0.001, ****P < 0.0001.

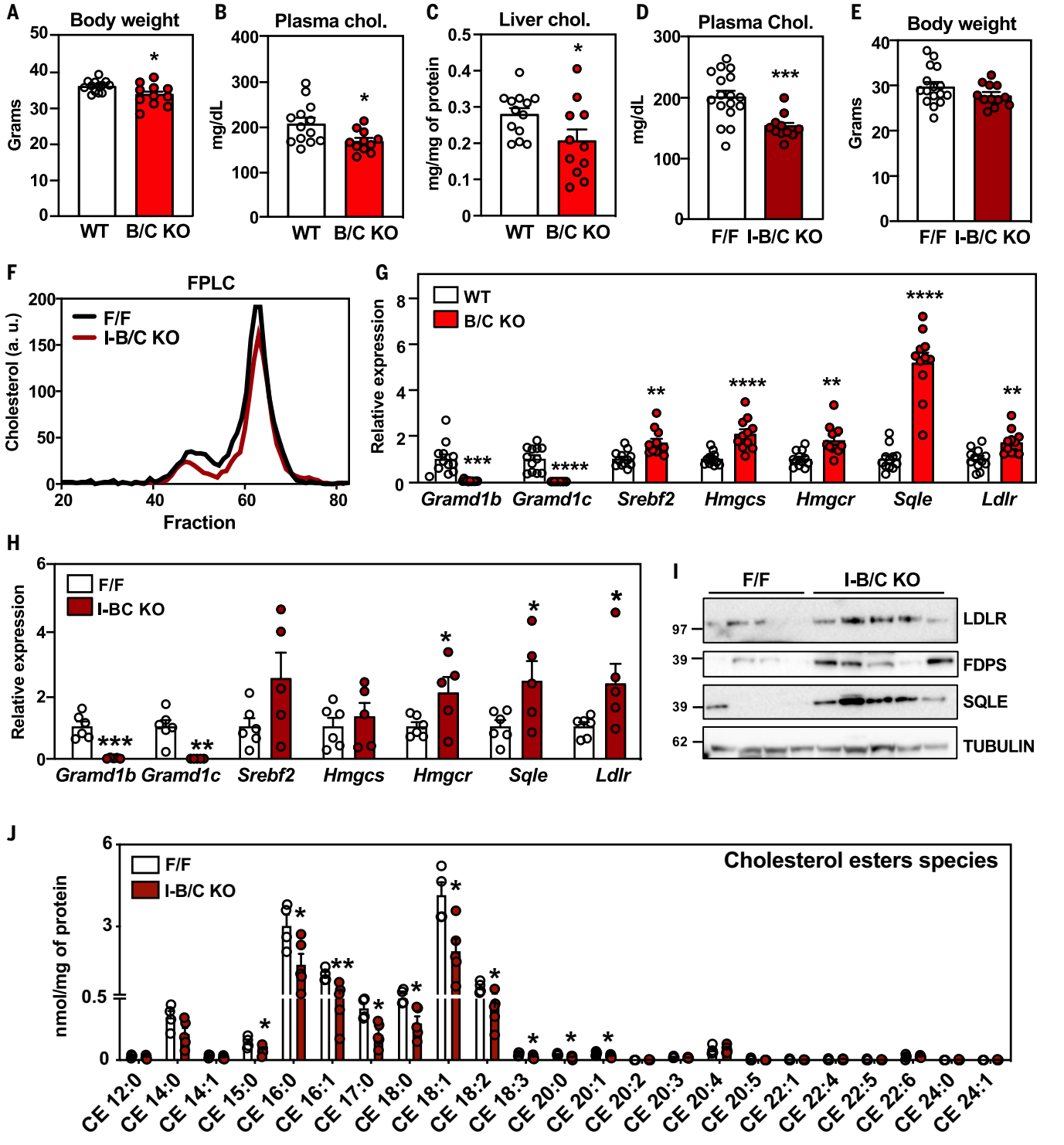

Fig. 4. Deletion of intestinal Asters protects from diet-induced hypercholesterolemia. (**A**) Body weight of WT (n = 13) and B/C KO (n = 11) male mice after 21 days of a Western diet plus 1.25% cholesterol (HC). (**B**) Plasma cholesterol levels after 4 hours fasting in mice described in (A). (**C**) Liver cholesterol in mice described in (A). (**D**) Plasma cholesterol levels after 4 hours fasting in F/F (n = 17) and I-B/C KO (n = 11) male mice after 21 days of the HC diet. (**E**) Body weight of mice described in (D). (**F**) FPLC of plasma from F/F and I-B/C KO mice fed for 21 days with HC diet and euthanized after overnight fasting followed by 2 hours of refeeding with the HC diet (pool of 3 to 5 mice per group). (**G**) Gene expression in distal jejunum scrapings from WT (n = 12) and B/C KO (n = 11) mice after 21 days of the HC diet, euthanized after 4 hours fasting. (**H**) Gene expression in distal jejunum scrapings from F/F (n = 6) and I-B/C KO (n = 5) male mice after 21 days of the HC diet, euthanized after 4 hours fasting. (**I**) Western blot analysis of duodenum scrapings of mice described in (H) (n = 4 to 5). (**J**) Lipidomic analysis of CE in proximal jejunum scrapings from mice described in (H) (n = 5 per group). Data are expressed as mean ± SEM. Statistical analysis: unpaired t test, $^{*}P < 0.05$, $^{**}P < 0.01$, $^{***}P < 0.001$, $^{****}P < 0.0001$.

Ezetimibe binds to Aster-B and Aster-C

Because both Aster deficiency and EZ reduce cholesterol absorption, we tested whether Asters might bind EZ. Using competition assays for 22-NBD-cholesterol binding, we found that EZ bound to Aster-B and Aster-C (Fig. 5A) with moderate affinity but exhibited minimal binding to Aster-A and StARD1 (fig. S8A). Next, we solved the crystal structure, at 1.6 Å resolution, of the ASTER domain from Aster-C complexed to EZ. The overall structure of the Aster-C domain revealed a canonical curved seven-stranded beta-sheet that forms a cavity to accommodate EZ (Fig. 5B and table S3). The cavity is closed by a long carboxyl-terminal helix and two shorter helices. The electron density map and the simulated annealing composite omit map highlighted additional volume within the binding cavity that accommodates a glycerol molecule, and density for part of a PEG4000 molecule from the cryo-protectant and crystallization buffer (fig. S8, B and C, respectively). The electron density for the PEG is stronger at the end in proximity to the EZ ligand and becomes weaker at the other end, presumably due to disorder. Thus, the precise translational position of the PEG is uncertain. Modeling of ezetimibe-glucuronide—the active metabolite of EZ—in the pocket suggested potential capacity for binding as the glucuronide group is oriented toward an opening of the pocket (fig. S8D). Circular dichroism (CD) spectra of the Aster-A, -B, and -C domains revealed that Aster-B and -C were thermally stabilized by EZ binding, whereas Aster-A was not (fig. S8E). Cholesterol and U18666A were included as positive controls (*25*, *36*).

To investigate the molecular basis for selective binding of EZ to Aster-C, we compared the structures of Aster-C:EZ and Aster-A:25–hydroxycholesterol (Fig. 5C). Many of the residues involved in ligand interactions are conserved in Aster-A and Aster-C (fig. S8F). However, leucine 400 and phenylalanine 405 in the ASTER domain of Aster-A appeared to represent a steric hindrance to EZ binding (Fig. 5D), whereas alanine 357 and isoleucine 362 in the ASTER domain of Aster-C left ample space for EZ binding (Fig. 5D). The importance of the specific amino acids on EZ binding was interrogated by mutagenesis and evaluation of thermal stability by CD. The two residues that appeared to hinder EZ binding in Aster-A were changed to the residues found in Aster-C (L400A_F405I). Conversely, the residues that appeared to be important for accommodating EZ binding in Aster-C were changed to those in Aster-A (A357L_I362F), which potentially prevent binding. The Aster-A mutant L400A_F405I, as well as the single mutant L400A, reduced Aster-A thermal stability (fig. S8G), but the stability was increased by EZ. The thermal stability upon EZ binding was unchanged in the F405I mutant (fig. S8G), suggesting that L400A is crucial for binding selectivity. These results were corroborated by the Aster-C mutants, where A357L_I362F and A357L alone increased thermal stability of the protein whereas I362F had no effect. The thermal stability of the A357L Aster-C mutant did not change with EZ binding, implying a weak interaction between EZ and that mutant (fig. S8G).

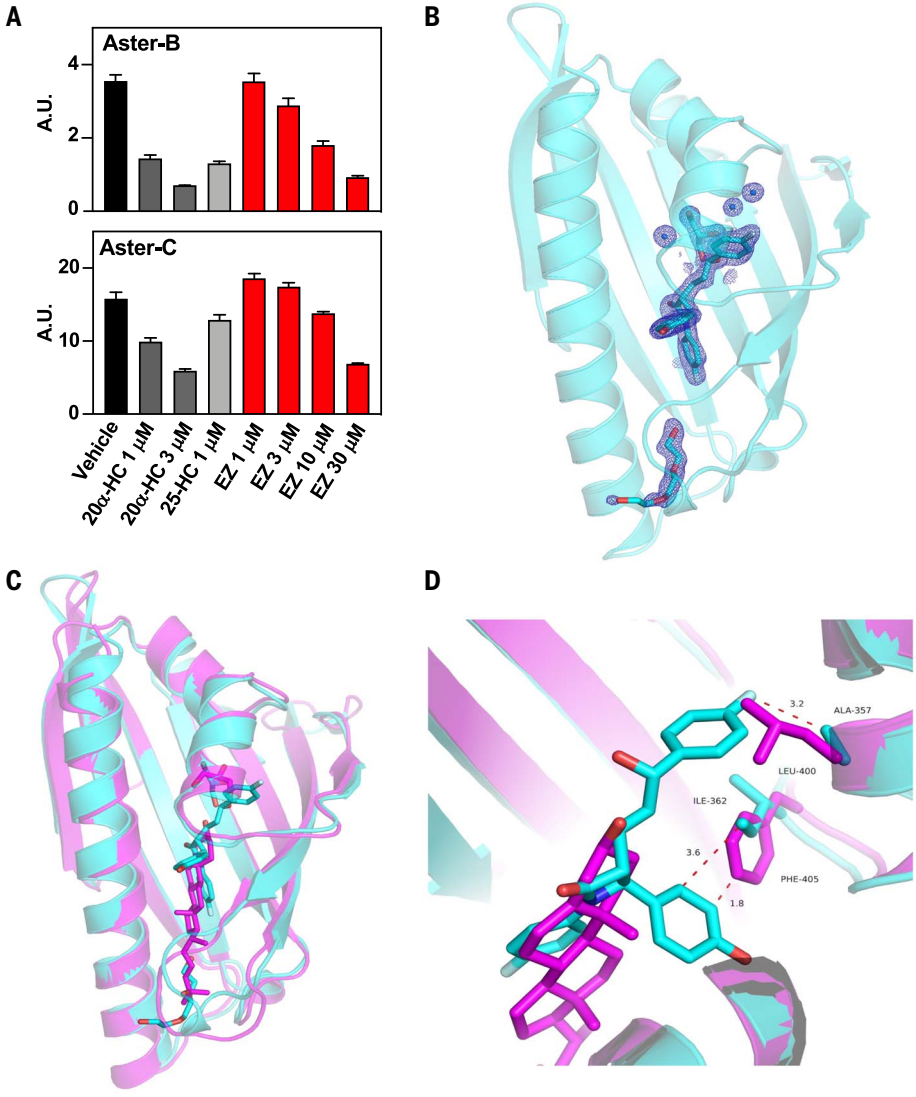

Fig. 5. Aster-B and Aster-C bind ezetimibe. (**A**) Competition assays for 22-NBD-cholesterol binding to purified ASTER-B and ASTER-C domains incubated in the presence of a vehicle, 20 α-HC, 25-HC, or EZ (1 to 30 mM). Data bars represent means ± SD. (**B**) Illustrated representation of the atomic structure at 1.6 Å resolution of the ASTER domain of Aster-C complexed to EZ. The EZ ligand in cyan sticks fits in a pocket created between the highly curved β-sheet, the second short helix, and the carboxyl-terminal helix. The cavity also accommodates glycerol (cyan sticks), water molecules (blue spheres), and part of a PEG 4000 molecule (cyan sticks). 2Fo-Fc electron density map of EZ, glycerol, part of PEG 4000, and water molecules in the binding cavity shown as blue mesh contoured at 1.2 σ. (**C**) Superposition of Aster-C:EZ (cyan) with the structure of Aster-A:25-HC (pdb ID 6GQF). The overall architecture of the domain is very similar but there are differences in the binding pocket and the opening loop. (**D**) Detail of the interaction between EZ and Aster-C involving residues ALA 357 and ILE 362, and superposition of the Aster-A:25-HC interaction. The superposition reveals how LEU 400 and PHE 405 from the Aster-A domain would clash with EZ, potentially preventing Aster-A from binding EZ.

Asters cooperate with NPC1L1 in intestinal cholesterol absorption

The ability of Aster-B and -C to bind EZ suggested that they may act in concert with NPC1L1 to promote cholesterol absorption. To test this hypothesis, we fed mice a moderate-cholesterol control diet or a moderate-cholesterol diet containing 0.01% EZ for 3 days (fig. S9A). As

expected, EZ decreased CE content and fractional cholesterol absorption by the fecal dual isotope method in WT mice (Fig. 6, A to C). Aster-B/C-KO and I-B/C-KO mice showed decreased CE content (Fig. 6, A and B) and fractional cholesterol absorption (Fig. 6C); EZ treatment led to a further reduction. Aster deficiency did not provide an additional decrease in CE or cholesterol absorption in EZ-treated mice (Fig. 6, A to C). However, gene expression and protein analyses revealed stronger activation of the SREBP-2 pathway in Aster-B/C-KO mice on the EZ diet compared with either Aster-B/C KO mice or EZ-treated WT mice (fig. S9B and Fig. 6D).

Cholesterol loading triggers Aster-B movement to the PM (Fig. 1B). EZ blocks the channel within NPC1L1 required for cholesterol deposition into the PM (*15*). Therefore, we theorized that EZ would attenuate Aster translocation to the PM by preventing the expansion of the accessible cholesterol pool. To test this idea, 3×HA-Aster-B mice were fed control or EZ diet for 3 days and gavaged with vehicle or EZ 30 min prior to a second gavage of cholesterol in corn oil. Small intestines were harvested 1 hour later. EZ completely prevented the recruitment of Aster-B to the brush border after cholesterol gavage (Fig. 6E). Next, we everted enteroids such that the apical PM was facing out (*37*) and administered mixed micelles (MM) containing cholesterol in the presence of vehicle or EZ. Immunofluorescence microscopy confirmed that recruitment of HA-Aster-B to the apical PM of enteroids was induced by cholesterol loading in MM but reduced by EZ (fig. S9C). Furthermore, we found decreased ALOD4 staining in enteroids derived from NPC1L1-KO mice loaded with MM cholesterol, indicating that NPC1L1 is required to saturate the PM with accessible cholesterol (Fig. 6F, upper panels). When enteroids were loaded with MβCD cholesterol, ALOD4 binding was not different between NPC1L1KO and WT enteroids (Fig. 6F, bottom panels). Thus, delivery of cholesterol in MβCD effectively bypasses the function of NPC1L1.

We then crossed 3×HA-Aster-B mice to NPC1L1 WT (HA-B-NPC1L1 WT) or NPC1L1 KO (HA-B-NPC1L1 KO) animals. In enteroids derived from these mice, NPC1L1 deletion reduced 3×HA-Aster-B recruitment to the PM after MM cholesterol loading but had no effect on MβCD cholesterol loading (fig. S9D). Analysis of HA-B-NPC1L1 WT and HA-B-NPC1L1 KO mice confirmed that genetic ablation of NPC1L1 abolished Aster-B movement to the brush border in response to cholesterol loading, mirroring the effects of EZ (Fig. 6G and fig. S9E). These results substantiate the hypothesis that EZ prevents Aster translocation to the brush border through NPC1L1 blockade. They further show that EZ prevents the saturation of cholesterol at the apical membrane by inhibiting NPC1L1 rather than Aster-B/C inhibition.

Next, we generated an McA-RH7777 CRL-1601 cell line stably expressing NPC1L1-EGFP and HA-Aster-B fusion proteins. Following cholesterol depletion, NPC1L1 partially localized to the PM, whereas Aster-B was confined to the ER (fig. S9F). MβCD-cholesterol loading caused internalization of NPC1L1-EGF and, concomitantly, the movement of HA-Aster-B to ER-PM contact sites. This contrasting behavior of NPC1L1 and Aster in response to cholesterol loading argues against a direct physical interaction between the two proteins during cholesterol import.

Pharmacological Aster inhibition reduces intestinal cholesterol uptake

Previous work from our laboratory identified a small molecule, AI-3d, that potently inhibits Aster-A, -B, and -C (*36*). We tested the ability of AI-3d to mimic the effects of Aster deficiency on cholesterol absorption. First, we pretreated enteroids with AI-3d and assessed accessible cholesterol with the ALOD4 probe. Treatment of WT enteroids with AI-3d and MβCD cholesterol led to an accumulation of accessible cholesterol, whereas AI-3d had no additional effect on ALOD4 binding in B/C-KO enteroids (Fig. 7A and fig. S10A). AI-3d generated a similar effect in human jejunal enteroids (Fig. 7B), indicating that AI-3d inhibits both human and murine Asters. We also compared the effects of AI-3d on WT and NPC1L1 KO enteroids. When enteroids were loaded with MM cholesterol, AI-3d treatment increased ALOD4 binding only in NPC1L1 WT cells (fig. S10B). However, when enteroids were loaded with MβCD-cholesterol, AI-3d treatment increased ALOD4 binding similarly in WT and NPC1L1 KO cells (fig. S10C). Thus, NPC1L1 deposits micellular cholesterol into the PM to expand the accessible pool and MβCD bypasses this function.

Finally, we assessed the impact of AI-3d on cholesterol transport to the ER. Consistent with our results in Aster-KO mice, AI-3d increased SREBP-2 target gene expression in human enteroids (Fig. 7C) and differentiated Caco-2 cells (fig. S10D). We further tested the effects of AI-3d on cholesterol absorption in vivo. C57BL/6J mice were pretreated with AI-3d or EZ for 1 hour, gavaged with [^{14}C]cholesterol, and given an intraperitoneal injection of Poloxamer-407. EZ treatment and pharmacologic inhibition of Asters both reduced dietary cholesterol absorption into the circulation (Fig. 7D).

Next, we evaluated the impact of Aster inhibition on mice fed a moderate-cholesterol diet (fig. S10E). AI-3d did not affect body weight or intestinal length (fig. S10, F to H), supporting the absence of toxicity. Lipidomic analysis revealed reduced CE in jejunal scrapings from NPC1L1 KO compared with WT mice. Aster inhibition by AI-3d lowered levels of jejunal CE similarly in WT and NPC1L1 KO, indicating that AI-3d does not act through NPC1L1 (Fig. 7E). Gene expression analysis showed a further induction of SREBP2 targets in NPC1L-KO mice treated with AI-3d (Fig. 7F).

Finally, we tested the effect of AI-3d on NPC1L1 recycling using McA-RH7777 CRL-1601 cells stably expressing an NPC1L1-EGFP fusion protein. Consistent with published data (*17*), we observed that NPC1L1-EGFP was present within a recycling compartment when both vehicle-treated and AI-3d treated cells were cultured in full serum (fig. S10I, left panels). In response to cholesterol depletion by MβCD, the signal in both cell types moved to the PM (fig. S10I, middle panels). Conversely, MβCD-cholesterol loading led to the relocation of NPC1L1-EGFP to endosomes (fig. S10I, right panels). These results indicate that AI-3d treatment does not interfere with the process of NPC1L1 recycling, further supporting the conclusion that AI-3d inhibits cholesterol absorption by targeting Asters.

Discussion

The involvement of NPC1L1 in facilitating the entry of cholesterol into enterocytes and the role of ACAT2 in cholesterol esterification are well documented and both proteins are recognized to be key players in the process of cholesterol absorption (*5*, *6*). However, how cholesterol that enters the cell through NPC1L1 reaches the ER for esterification and regulation of cholesterol synthesis has been a long-standing mystery. Here we solve that mystery by showing that Aster-B and -C link NPC1L1 to ACAT2 by facilitating nonvesicular cholesterol transport to the ER following uptake by NPC1L1 at the enterocyte PM. Combined deletion of Aster-B and -C impairs the movement of dietary cholesterol to ER in enterocytes, as evidenced by expansion of the accessible PM cholesterol pool, reduced CE formation, and activation of the SREBP-2 pathway for cholesterol synthesis. Physiologically, inhibition of Aster nonvesicular transport reduces cellular cholesterol stores and impairs the incorporation of CE into chylomicrons.

Our results suggest that cholesterol homeostasis in enterocytes requires both NPC1L1-mediated cholesterol deposition into the PM and subsequent Aster-mediated transport to the ER. Because NPC1L1 is the gatekeeper that controls the first step of cholesterol uptake, cholesterol absorption is reduced when NPC1L1 is blocked by EZ. In this context, Aster deletion does not further decrease absorption, because the apical PM cholesterol available for transfer is limited. At the same time, the observation that CE production in the ER is markedly impaired by Aster deletion even when NPC1L1 is present argues against a dominant role for NPC1L1 itself in cholesterol transport to the ER. Thus, NPC1L1 and Asters function in series to move cholesterol from the diet into circulation. EZ binds to Aster-B

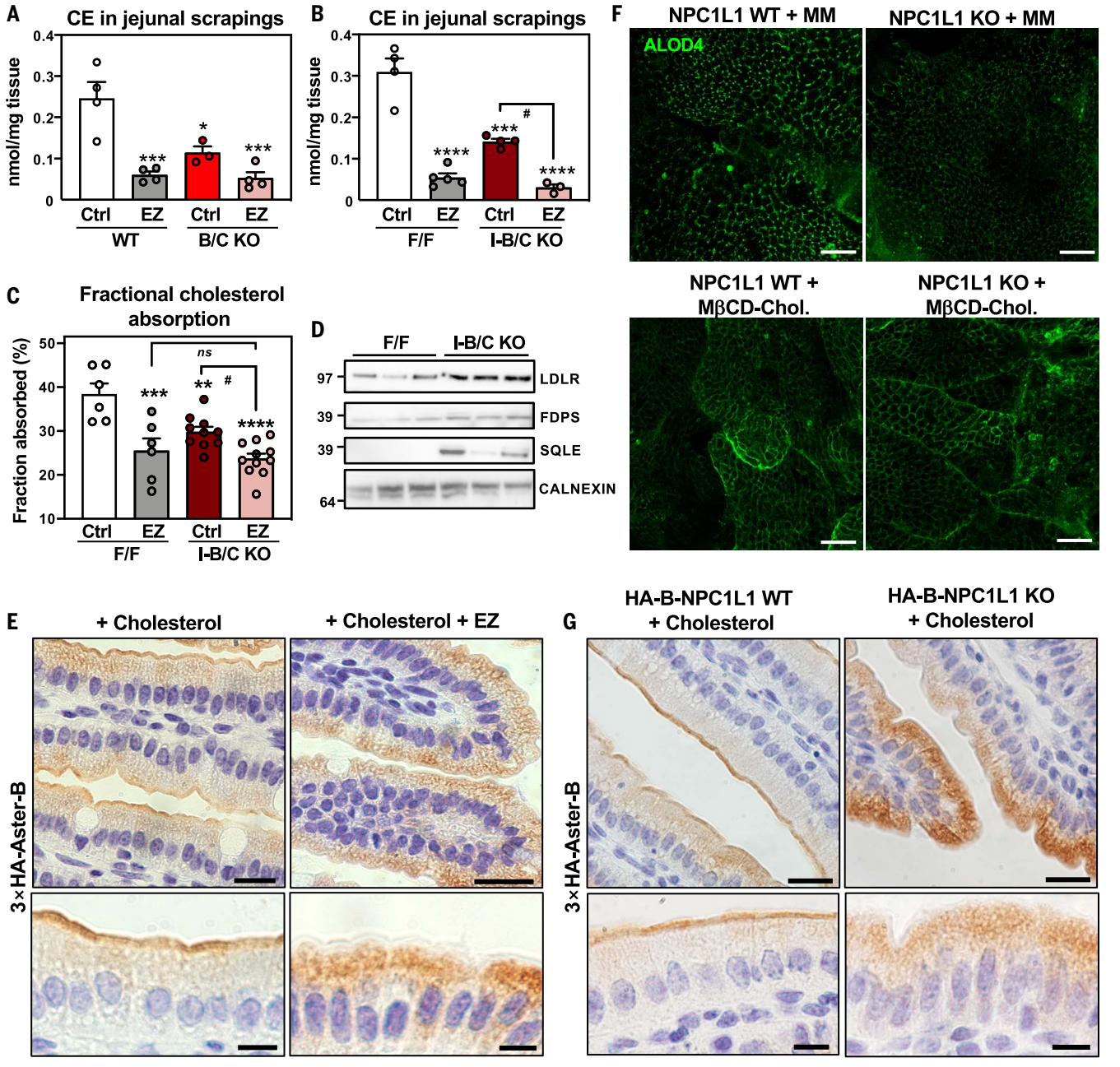

Fig. 6. NPC1L1 enriches accessible cholesterol at the brush border and promotes Aster recruitment. (**A**) CE quantification by mass spectrometry in scrapings from proximal jejunum of WT and B/C KO mice fed for 3 days with a control diet (ctrl) containing 0.08% cholesterol or a diet containing 0.08% cholesterol and 0.01% EZ and euthanized after 10 hours fasting followed by 2 hours refeeding with the same diets (n = 3 to 5 per group). (**B**) CE quantification by mass spectrometry in scrapings from proximal jejunum of F/F and I-B/C KO mice fed for 3 days with a control diet (ctrl) containing 0.08% cholesterol or a diet containing 0.08% cholesterol and 0.01% EZ) and euthanized 2 hours after refeeding (n = 3 to 5 per group). (**C**) Fractional absorption of cholesterol measured by the fecal dual isotope method in F/F and I-B/C KO mice fed for 3 days with a control diet (ctrl) containing 0.08% cholesterol or a diet containing 0.08% cholesterol and 0.01% EZ. (**D**) Western blot analysis of duodenum scrapings from F/F and I-B/C KO mice fed for 3 days with EZ diet (n = 3 per group). Samples were run on the same gel used for Western blot analysis reported in fig. S3F; therefore the loading control (Calnexin) is the same. (**E**) Immunohistochemistry of HA-Aster-B in small intestines from 3×HA-Aster-B mice after oral administration of vehicle or EZ and a gastric gavage with cholesterol in corn oil. (**F**) ALOD4 imaging of murine enteroids from WT and NPC1L1 KO mice after loading with cholesterol in mixed micelles or with MβCD-cholesterol. Scale bar is 40 μm. (**G**) Immunohistochemistry of HA-Aster-B in small intestines from 3×HA-Aster-B mice crossed to NPC1L1 WT or NPC1L1 KO mice after a gastric gavage with cholesterol in corn oil. For (E) and (G) upper and lower panels, scale bar is 20 and 10 μm, respectively. Data are expressed as mean ± SEM. 2-way ANOVA with Tukey's multiple comparisons test. Data are expressed as mean ± SEM. $^{*}P < 0.05$, $^{**}P < 0.01$, $^{***}P < 0.001$, $^{****}P < 0.0001$ versus WT Ctrl, $^{\#}P < 0.05$ versus I-B/C KO Ctrl.

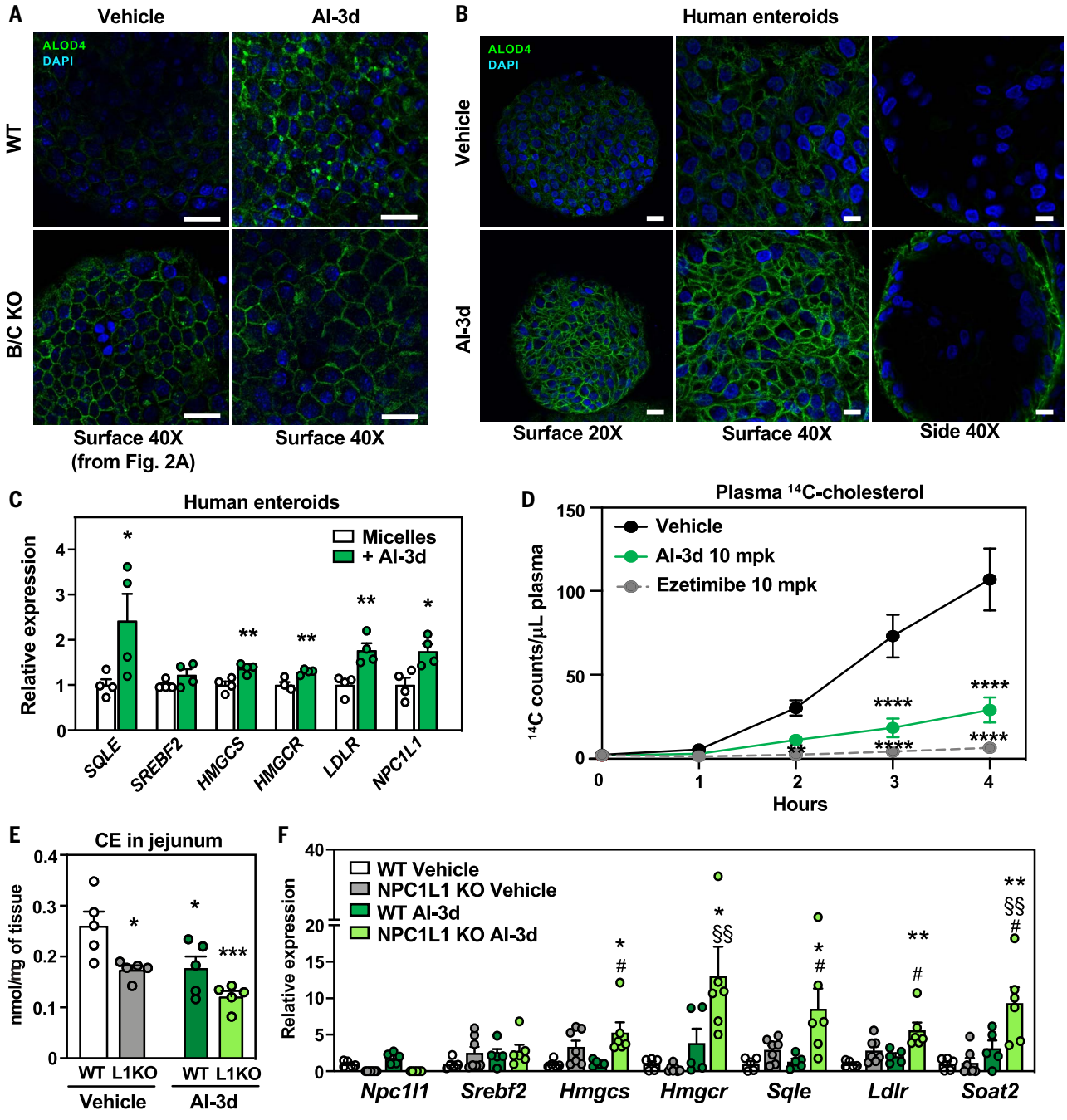

Fig. 7. Pharmacological inhibition of Asters reduces intestinal cholesterol uptake. (**A**) ALOD4 staining (green) of PM accessible cholesterol in enteroids from WT and B/C KO mice loaded with MβCD cholesterol and treated with vehicle or Aster inhibitor Al-3d. Results presented in this panel and in Fig. 2C came from one experiment, where WT vehicle-treated enteroids served as control for both B/C KO vehicle-treated enteroids and for Al-3d vehicle-treated enteroids. Scale bar is 20 µm. (**B**) ALOD4 staining (green) of PM accessible cholesterol in human enteroids treated with vehicle or Al-3d. For left panels, scale bar is 20 µm. For middle and right panels, scale bar is 10 µm. (**C**) Gene expression of SREBP-2 and target genes in human enteroids differentiated on transwell plates and loaded with cholesterol in mixed micelles in the presence of vehicle or Al-3d. (**D**) Kinetics of radioactivity in plasma of female mice that were administered vehicle (n = 6), Al-3d (n = 5), or EZ (n = 6) in corn oil. After 1 hour, the mice were given a gastric gavage of olive oil containing [^{14}C]cholesterol. (**E**) CE quantification by mass spectrometry in scrapings from proximal jejunum of NPC1L1 WT and NPC1L1 KO mice fed for 3 days with a control diet (ctrl) containing 0.08% cholesterol and treated with 3 doses of vehicle (left) or 10 mg/kg Al-3d (right) and euthanized after 10 hours of fasting followed by 2 hours refeeding with the same diet (n = 5 per group). (**F**) Gene expression analysis of distal jejunum scrapings from mice described in (E). Statistical analysis for (C), unpaired t test; for s, (D), (E), (F), 2-way ANOVA with Tukey's multiple comparisons test. Data are expressed as mean ± SEM. For (C), $^{*}P < 0.05$, $^{**}P < 0.01$ versus micelles. For (D) $^{**}P < 0.01$, $^{****}P < 0.0001$ versus Vehicle. For s (D), (E) $^{*}P < 0.05$, $^{**}P < 0.01$ versus WT Vehicle, $^{\#}P < 0.05$ versus WT Al-3d, $^{\S\S}P < 0.01$ versus NPC1L1 KO Vehicle.

and -C with moderate affinity, raising the possibility that inhibition of Aster function could contribute to EZ's capacity to inhibit cholesterol absorption. However, EZ binding to Aster was not sufficient to block nonvesicular cholesterol transport in vivo in our studies, as Aster deletion further reduced ER cholesterol delivery in the presence of EZ.

The recruitment of Asters to the PM depends on the cholesterol and phosphatidylserine content in the inner leaflet (*25*, *26*, *33*). Our results support the notion that Aster-mediated nonvesicular transport relies on NPC1L1 to deposit cholesterol into the apical enterocyte PM, rather than on a direct physical interaction with NPC1L1. In support of this concept, micelle-derived cholesterol cannot contribute to the expansion of the accessible pool, and Aster proteins do not translocate to the enterocyte PM when NPC1L1 is deleted or inhibited by EZ. However, when NPC1L1 is bypassed by delivering cholesterol directly to the PM with MβCD, Aster is recruited normally.

Previous studies have demonstrated that NPC1L1 is internalized when enterocytes are exposed to dietary cholesterol (*38*). This observation has led to the suggestion that vesicular transport by NPC1L1-containing vesicles is important for cholesterol delivery to the ER (*21*, *24*, *38*). However, formal tests of the relative contribution of vesicular and nonvesicular cholesterol transport mechanisms downstream of NPC1L1 have been lacking. Our data indicate that the primary function of NPC1L1 is to deposit dietary cholesterol into the enterocyte PM. NPC1L1 is a homolog of the Niemann-Pick C1 (NPC1) protein that mediates cholesterol export from lysosomes following endocytosis of LDL cholesterol (*39*). Molecular studies have established that NPC1 acts to enrich cholesterol in the lysosomal membrane (*40*, *41*), and that such enrichment allows for the subsequent transfer of cholesterol to PM by cytoplasmic nonvesicular transfer proteins (*42*). Our results suggest that the structurally related NPC1 and NPC1L1 perform analogous functions: both enrich membrane cholesterol to facilitate the recruitment of nonvesicular transporters. We propose that the sterol-regulated endocytosis of NPC1L1 could represent a feedback mechanism to limit cholesterol absorption, rather than a major mechanism for vesicular cholesterol transfer to the ER. However, our data do not exclude the participation of other vesicular and nonvesicular pathways in the intracellular movement of cholesterol in enterocytes. Nor do they exclude the possibility that Aster proteins retrieve cholesterol, directly or indirectly, from NPC1L1-rich endosomes.

Intestinal nonvesicular cholesterol transport could be a target for treating diet-induced hypercholesterolemia. First, Aster-B/C knockout mice have low plasma cholesterol levels when fed a Western diet enriched in cholesterol. Second, we showed that the Aster pathway can be targeted pharmacologically to reduce cholesterol absorption. The inhibitor AI-3d, which had been shown previously (*36*) to inhibit Aster-mediated nonvesicular transport in vitro, reduced cholesterol transport to the ER and expanded the pool of accessible cholesterol at the PM of intestinal enteroids. Finally, treatment of mice with AI-3d diminished cholesterol absorption. These findings identify the Aster pathway as a potentially attractive pathway for limiting intestinal cholesterol absorption and reducing plasma cholesterol.

Materials and methods summary

Detailed materials and methods can be found in the supplementary materials (*43*), including generation of murine models, experimental conditions for in vivo studies, histology and immunohistochemistry, cholesterol absorption assays, lipid measurements, chylomicron isolation, isolation of intestinal epithelial cells, protein isolation and immunoblot assays, RNA extraction and gene expression analysis, in vivo back-scattered electron (BSE) microscopy and NanoSIMS, isolation of murine crypts, culture and expansion of enteroids (basolateral-out or apical-out), culture of human intestinal epithelial cells on transwell membranes for gene expression, immunofluorescence microscopy, purification and fluorophore conjugation of ALOD4, immortalized cell cultures (Caco-2 and McArdle RH7777), protein expression and purification, crystallization and x-ray structure determination, and circular dichroism.

REFERENCES AND NOTES

1. P. Xie *et al*., Genetic demonstration of intestinal NPC1L1 as a major determinant of hepatic cholesterol and blood atherogenic lipoprotein levels. *Atherosclerosis* **237**, 609–617 (2014). doi: 10.1016/j.atherosclerosis.2014.09.036; pmid: 25463095
2. C. M. Mansbach, S. A. Siddiqi, The biogenesis of chylomicrons. *Annu. Rev. Physiol.* **72**, 315–333 (2010). doi: 10.1146/annurev-physiol-021909-135801; pmid: 20148678
3. K. K. Buhman *et al*., Resistance to diet-induced hypercholesterolemia and gallstone formation in ACAT2-deficient mice. *Nat. Med.* **6**, 1341–1347 (2000). doi: 10.1038/82153; pmid: 11100118
4. T. M. Nguyen, J. K. Sawyer, K. L. Kelley, M. A. Davis, L. L. Rudel, Cholesterol esterification by ACAT2 is essential for efficient intestinal cholesterol absorption: Evidence from thoracic lymph duct cannulation. *J. Lipid Res.* **53**, 95–104 (2012). doi: 10.1194/jlr.M018820; pmid: 22045928
5. J. Zhang *et al*., Tissue-specific knockouts of ACAT2 reveal that intestinal depletion is sufficient to prevent diet-induced cholesterol accumulation in the liver and blood. *J. Lipid Res.* **53**, 1144–1152 (2012). doi: 10.1194/jlr.M024356; pmid: 22460046
6. S. W. Altmann *et al*., Niemann-Pick C1 Like 1 protein is critical for intestinal cholesterol absorption. *Science* **303**, 1201–1204 (2004). doi: 10.1126/science.1093131; pmid: 14976318
7. H. R. Davis Jr. *et al*., Niemann-Pick C1 Like 1 (NPC1L1) is the intestinal phytosterol and cholesterol transporter and a key modulator of whole-body cholesterol homeostasis. *J. Biol. Chem.* **279**, 33586–33592 (2004). doi: 10.1074/jbc.M405817200; pmid: 15173162
8. M. Garcia-Calvo *et al*., The target of ezetimibe is Niemann-Pick C1-Like 1 (NPC1L1). *Proc. Natl. Acad. Sci. U.S.A.* **102**, 8132–8137 (2005). doi: 10.1073/pnas.0500269102; pmid: 15928087
9. H. R. Davis Jr., K. K. Pula, K. B. Alton, R. E. Burrier, R. W. Watkins, The synergistic hypocholesterolemic activity of the potent cholesterol absorption inhibitor, ezetimibe, in combination with 3-hydroxy-3-methylglutaryl coenzyme a reductase inhibitors in dogs. *Metabolism* **50**, 1234–1241 (2001). doi: 10.1053/meta.2001.26737; pmid: 11586500
10. C. P. Cannon *et al*., Ezetimibe Added to Statin Therapy after Acute Coronary Syndromes. *N. Engl. J. Med.* **372**, 2387–2397 (2015). doi: 10.1056/NEJMoa1410489; pmid: 26039521
11. J. W. Clader, The discovery of ezetimibe: A view from outside the receptor. *J. Med. Chem.* **47**, 1–9 (2004). doi: 10.1021/jm030283g; pmid: 14695813
12. H. R. Davis Jr., D. S. Compton, L. Hoos, G. Tetzloff, Ezetimibe, a potent cholesterol absorption inhibitor, inhibits the development of atherosclerosis in ApoE knockout mice. *Arterioscler. Thromb. Vasc. Biol.* **21**, 2032–2038 (2001). doi: 10.1161/hq1201.100260; pmid: 11742881
13. R. G. Lee *et al*., Plasma cholesteryl esters provided by lecithin: cholesterol acyltransferase and acyl-coenzyme a:cholesterol acyltransferase 2 have opposite atherosclerotic potential. *Circ. Res.* **95**, 998–1004 (2004). doi: 10.1161/01.RES.0000147558.15554.67; pmid: 15486318
14. M. Hu *et al*., Structural insights into the mechanism of human NPC1L1-mediated cholesterol uptake. *Sci. Adv.* **7**, eabg3188 (2021). doi: 10.1126/sciadv.abg3188; pmid: 34272236
15. C.-S. Huang *et al*., Cryo-EM structures of NPC1L1 reveal mechanisms of cholesterol transport and ezetimibe inhibition. *Sci. Adv.* **6**, eabb1989 (2020). doi: 10.1126/sciadv.abb1989; pmid: 34407950
16. T. Long, Y. Liu, Y. Qin, R. A. DeBose-Boyd, X. Li, Structures of dimeric human NPC1L1 provide insight into mechanisms for cholesterol absorption. *Sci. Adv.* **7**, eabh3997 (2021). doi: 10.1126/sciadv.abh3997; pmid: 34407950
17. L. Ge *et al*., The cholesterol absorption inhibitor ezetimibe acts by blocking the sterol-induced internalization of NPC1L1. *Cell Metab.* **7**, 508–519 (2008). doi: 10.1016/j.cmet.2008.04.001; pmid: 18522832
18. A. B. Weinglass *et al*., Extracellular loop C of NPC1L1 is important for binding to ezetimibe. *Proc. Natl. Acad. Sci. U.S.A.* **105**, 11140–11145 (2008). doi: 10.1073/pnas.0800936105; pmid: 18682566
19. L. Ge *et al*., Flotillins play an essential role in Niemann-Pick C1-like 1-mediated cholesterol uptake. *Proc. Natl. Acad. Sci. U.S.A.* **108**, 551–556 (2011). doi: 10.1073/pnas.1014434108; pmid: 21187433
20. L.-J. Wang *et al*., Molecular characterization of the NPC1L1 variants identified from cholesterol low absorbers. *J. Biol. Chem.* **286**, 7397–7408 (2011). doi: 10.1074/jbc.M110.178368; pmid: 21189420
21. P.-S. Li *et al*., The clathrin adaptor Numb regulates intestinal cholesterol absorption through dynamic interaction with NPC1L1. *Nat. Med.* **20**, 80–86 (2014). doi: 10.1038/nm.3417; pmid: 24336247
22. B.-B. Chu *et al*., Requirement of myosin Vb.Rab11a.Rab11-FIP2 complex in cholesterol-regulated translocation of NPC1L1 to the cell surface. *J. Biol. Chem.* **284**, 22481–22490 (2009). doi: 10.1074/jbc.M109.034355; pmid: 19542231
23. T. A. Johnson, S. R. Pfeffer, Ezetimibe-sensitive cholesterol uptake by NPC1L1 protein does not require endocytosis. *Mol. Biol. Cell* **27**, 1845–1852 (2016). doi: 10.1091/mbc.e16-03-0154; pmid: 27075173
24. Y.-Y. Zhang *et al*., A *LIMA1* variant promotes low plasma LDL cholesterol and decreases intestinal cholesterol absorption. *Science* **360**, 1087–1092 (2018). doi: 10.1126/science.aao6575; pmid: 29880681
25. J. Sandhu *et al*., Aster Proteins Facilitate Nonvesicular Plasma Membrane to ER Cholesterol Transport in Mammalian Cells. *Cell* **175**, 514–529.e20 (2018). doi: 10.1016/j.cell.2018.08.033; pmid: 30220461
26. T. Naito *et al*., Movement of accessible plasma membrane cholesterol by the GRAMD1 lipid transfer protein complex. *eLife* **8**, e51401 (2019). doi: 10.7554/eLife.51401; pmid: 31724953
27. M. Besprozvannaya *et al*., GRAM domain proteins specialize functionally distinct ER-PM contact sites in human cells. *eLife* **7**, e31019 (2018). doi: 10.7554/eLife.31019; pmid: 29469807
28. X. Xiao *et al*., Hepatic nonvesicular cholesterol transport is critical for systemic lipid homeostasis. *Nat. Metab.* **5**, 165–181 (2023). doi: 10.1038/s42255-022-00722-6; pmid: 36646756
29. B. Wang, P. Tontonoz, Liver X receptors in lipid signalling and membrane homeostasis. *Nat. Rev. Endocrinol.* **14**, 452–463 (2018). doi: 10.1038/s41574-018-0037-x; pmid: 29904174
30. L. Yu *et al*., Expression of ABCG5 and ABCG8 is required for regulation of biliary cholesterol secretion. *J. Biol. Chem.* **280**, 8742–8747 (2005). doi: 10.1074/jbc.M411080200; pmid: 15611112
31. H. Jiang *et al*., High-resolution imaging of dietary lipids in cells and tissues by NanoSIMS analysis. *J. Lipid Res.* **55**, 2156–2166 (2014). doi: 10.1194/jlr.M053363; pmid: 25143463

32. C. He *et al*., NanoSIMS Analysis of Intravascular Lipolysis and Lipid Movement across Capillaries and into Cardiomyocytes. *Cell Metab.* **27**, 1055–1066.e3 (2018). doi: 10.1016/j.cmet.2018.03.017; pmid: 29719224
33. A. Ferrari *et al*., Aster Proteins Regulate the Accessible Cholesterol Pool in the Plasma Membrane. *Mol. Cell. Biol.* **40**, e00255–e00220 (2020). doi: 10.1128/MCB.00255-20; pmid: 32719109
34. A. Das, M. S. Brown, D. D. Anderson, J. L. Goldstein, A. Radhakrishnan, Three pools of plasma membrane cholesterol and their relation to cholesterol homeostasis. *eLife* **40**, e02882 (2014). doi: 10.1128/MCB.00255-20; pmid: 32719109
35. A. Gay, D. Rye, A. Radhakrishnan, Switch-like responses of two cholesterol sensors do not require protein oligomerization in membranes. *Biophys. J.* **108**, 1459–1469 (2015). doi: 10.1016/j.bpj.2015.02.008; pmid: 25809258
36. X. Xiao *et al*., Selective Aster inhibitors distinguish vesicular and nonvesicular sterol transport mechanisms. *Proc. Natl. Acad. Sci. U.S.A.* **118**, e2024149118 (2021). doi: 10.1073/pnas.2024149118; pmid: 33376205
37. J. Y. Co *et al*., Controlling Epithelial Polarity: A Human Enteroid Model for Host-Pathogen Interactions. *Cell Rep.* **26**, 2509–2520.e4 (2019). doi: 10.1016/j.celrep.2019.01.108; pmid: 30811997
38. C. Xie *et al*., Ezetimibe blocks the internalization of NPC1L1 and cholesterol in mouse small intestine. *J. Lipid Res.* **53**, 2092–2101 (2012). doi: 10.1194/jlr.M027359; pmid: 22811412
39. E. D. Carstea *et al*., Niemann-Pick C1 disease gene: Homology to mediators of cholesterol homeostasis. *Science* **277**, 228–231 (1997). doi: 10.1126/science.277.5323.228; pmid: 9211849
40. H. J. Kwon *et al*., Structure of N-terminal domain of NPC1 reveals distinct subdomains for binding and transfer of cholesterol. *Cell* **137**, 1213–1224 (2009). doi: 10.1016/j.cell.2009.03.049; pmid: 19563754
41. H. Qian *et al*., Structural Basis of Low-pH-Dependent Lysosomal Cholesterol Egress by NPC1 and NPC2. *Cell* **182**, 98–111.e18 (2020). doi: 10.1016/j.cell.2020.05.020; pmid: 32544384
42. H. Wang *et al*., ORP2 Delivers Cholesterol to the Plasma Membrane in Exchange for Phosphatidylinositol 4, 5-Bisphosphate (PI(4,5)P_2). *Mol. Cell* **73**, 458–473.e7 (2019). doi: 10.1016/j.molcel.2018.11.014; pmid: 30581148
43. Materials and methods are available as supplementary materials.

ACKNOWLEDGMENTS

We thank L. Fong, P. Kim, and E. Tokhtaeva for the technical assistance. We also thank members of the Tontonoz, Tarling-Vallim, Edwards, Villanueva, Young, and Bensinger labs at UCLA for useful advice and discussions and for sharing reagents and resources. We thank G. Su and the UCLA Lipidomics and Y. Li and the UCLA Translational Pathology Core Laboratory. pALOD4 was a gift from Arun Radhakrishnan (Addgene plasmids # 111026). We thank B.-L. Song at Wuhan University for the NPC1L1-EGFP construct and NPC1L1 KO mice. We thank T. Darwish for supporting the production of [2H]cholesterol. **Funding:** This work was supported by the following: National Institutes of Health grant R01 DK126779 (to P.T.); National Institutes of Health grant P01 HL146358 (to S.G.Y.); Transatlantic Network of Excellence, Leducq Foundation, 19CDV04; American Diabetes Association Postdoctoral fellowship 1-19-PDF-043-RA and Ermenegildo Zegna Founder's Scholarship 2017 (to A.F.); CDI Junior Faculty Career Development Award (CD-JFCD-07012019), CDI NIH K12 Junior Faculty Career Development Grant (CDI-K12-07012023), and Today's and Tomorrow's Children Fund Bridge Grant (CDI-TTCF-07012022) (to E.W.); UCSD-UCLA Diabetes Research Center (DK063491) (to E.W. and P.T.); American Heart Association Postdoctoral Fellowship 18POST34030388 to (X.X.); American Heart Association Postdoctoral Fellowship 903306 to (J.P.K.); the Damon Runyon Cancer Research Fellowship (DRG-2424-21) to (Y.G.); National Institutes of Health grant T32 DK007180 to (A.N.); and the National Collaborative Research Infrastructure Strategy (NCRIS), an Australian Government initiative, to the National Deuteration Facility in Australia. **Author contributions:** Conceptualization: A.F., E.W., and P.T. Methodology: A.F., E.W., X.X., J.P.K., S.D.L., A.N., T.W., L.F., M.G.M., R.A.R., L.C., A.B., K.W. Investigation: A.F., E.W., X.X., J.P.K., B.R.A., J.J.M., T.W., K.C., J.S., M.J.T., L.B., A.N., Y.K., Y.G., P.M., and W.S. Visualization: A.F., E.W., and P.T. Funding acquisition: S.G.Y. and P.T. Project administration: P.T. Supervision: M.E.J., H.J., J.W.R.S., S.G.Y., and P.T. Writing – original draft: A.F., E.W., and P.T. Writing – review and editing: A.F., E.W., M.E.J., H.J., J.W.R.S., S.G.Y., P.T. **Competing interests:** All authors declare that they have no competing interests. **Data and materials availability:** Source data for all figures are provided with the paper. Sequencing data have been deposited to GEO (GSE206780). The crystal structure has been submitted to the PDB database, PDB ID code 8AXW. All unique biological materials used are readily available from the authors or from standard commercial sources.

SUPPLEMENTARY MATERIALS

Submitted 28 September 2022; resubmitted 3 July 2023
Accepted 27 September 2023
10.1126/science.adf0966